

Production asymmetry of ν_τ neutrinos and $\bar{\nu}_\tau$ antineutrinos from a fixed target experiment SHiP

Rafał Maciuła,^{1,*} Antoni Szczurek^{†,1,‡} Jakub Zaremba,^{1,§} and Izabela Babiarcz^{1,¶}

¹*Institute of Nuclear Physics, Polish Academy of Sciences,
ul. Radzikowskiego 152, PL-31-342 Kraków, Poland*

Abstract

We discuss how to calculate cross sections as well as rapidity, transverse momentum and energy distributions of ν_τ and $\bar{\nu}_\tau$ produced from the direct $D_s^\pm \rightarrow \nu_\tau/\bar{\nu}_\tau$ and chain $D_s^\pm \rightarrow \tau^\pm/\tau^\mp \rightarrow \nu_\tau/\bar{\nu}_\tau$ decays in $p+^{96}\text{Mo}$ scattering with proton beam $E_{\text{lab}} = 400$ GeV *i.e.* at $\sqrt{s_{NN}} = 27.4$ GeV. The τ decays are simulated with the help of the TAUOLA code and include multiple decay channels of τ in amounts proportional to their branching ratios. In our calculations we include D_s^\pm from charm fragmentation $c \rightarrow D_s^+$ and $\bar{c} \rightarrow D_s^-$ as well as those from subleading fragmentation of strange quarks/antiquarks $s \rightarrow D_s^-$ and $\bar{s} \rightarrow D_s^+$. The $s \neq \bar{s}$ asymmetry of the strange quark content of proton is included. The different contributions to D_s^\pm and $\nu_\tau/\bar{\nu}_\tau$ are shown explicitly. We discuss and quantify a not discussed so far effect of asymmetries for production of ν_τ and $\bar{\nu}_\tau$ caused by subleading fragmentation mechanism and discuss related uncertainties. A potential measurement of the asymmetry is discussed. Estimates of a number of observed $\nu_\tau/\bar{\nu}_\tau$ in the $\nu_\tau/\bar{\nu}_\tau + ^{208}\text{Pb}$ reaction, with 2m long target are given with the help of the NuWro program. We refer also to the production of the high-energy (anti)neutrinos in the atmosphere.

[†] also at University of Rzeszów, PL-35-959 Rzeszów, Poland

^{*}Electronic address: rafal.maciula@ifj.edu.pl

[‡]Electronic address: antoni.szczurek@ifj.edu.pl

[§]Electronic address: jakub.zaremba@ifj.edu.pl

[¶]Electronic address: izabela.babiarz@ifj.edu.pl

I. INTRODUCTION

The ν_τ and $\bar{\nu}_\tau$ particles were ones of last ingredients of the Standard Model discovered experimentally [1]. So far only a few $\nu_\tau/\bar{\nu}_\tau$ neutrinos/antineutrinos were observed experimentally [2, 3]. Recently the IceCube experiment observed 2 cases of the τ neutrinos/antineutrinos [4].

The proposed SHiP (Search for Hidden Particles) experiment [5, 6] may change the situation [7]. It was roughly estimated that about 300 – 1000 neutrinos ($\nu_\tau + \bar{\nu}_\tau$) will be observed by the SHiP experiment [7, 8]. This will considerably improve our knowledge in this weakly tested corner of the Standard Model.

The $\nu_\tau/\bar{\nu}_\tau$ neutrinos/antineutrinos are known to be primarily produced from D_s^\pm decays. The corresponding branching fraction is relatively well known [9] and is $\text{BR}(D_s^\pm \rightarrow \tau^\pm) = 0.0548$. The D_s mesons are abundantly produced in proton-proton collisions. They were measured *e.g.* at the LHC by the ALICE [10] and the LHCb experiments [11]. The LHCb experiment in the collider-mode has observed even a small asymmetry in the production of D_s^+ and D_s^- [12]. So far the asymmetry is not fully understood from first principles. In Ref. [13] two of us proposed a possible explanation of the fact in terms of subleading $s \rightarrow D_s^-$ or $\bar{s} \rightarrow D_s^+$ fragmentations. However, the corresponding fragmentation functions are not well known.

Here we wish to investigate possible consequences for forward production of D_s mesons and forward production of ν_τ neutrinos and $\bar{\nu}_\tau$ antineutrinos. In our model D_s^\pm mesons can be produced from both, charm and strange quark/antiquark fragmentation, with a similar probability of the transition. The $s \rightarrow D_s$ mechanism is expected to be especially important at large rapidities (or large Feynman x_F) [13]. Does it has consequences for forward production of neutrinos/antineutrinos for the SHiP experiment? We shall analyze this issue in the present paper. In short, we wish to make as realistic as possible predictions of the cross section for production of $\nu_\tau/\bar{\nu}_\tau$ neutrinos/antineutrinos. Here we will also discuss interactions of the neutrinos/antineutrinos with the matter (Pb target was proposed for identifying neutrinos/antineutrinos). This was discussed already in the literature (see *e.g.* Ref. [14] and references therein).

II. SOME DETAILS OF THE APPROACH

Here we discuss in short mechanisms of production of D_s mesons, weak decays of D_s mesons to $\nu_\tau/\bar{\nu}_\tau$ neutrinos/antineutrinos and interactions of $\nu_\tau/\bar{\nu}_\tau$ neutrinos/antineutrinos with nuclear targets.

A. D_s meson production

In the present paper we discuss two mechanisms of D_s meson production:

- $c \rightarrow D_s^+, \bar{c} \rightarrow D_s^-$, called leading fragmentation,
- $\bar{s} \rightarrow D_s^+, s \rightarrow D_s^-$, called subleading fragmentation.

The underlying leading-order pQCD partonic mechanisms for charm and strange quark production are shown schematically in Fig. 1 and Fig. 2, respectively. At high energies, for charm quark production higher-order (NLO and even NNLO) corrections are very important, especially when considering differential distributions, such as quark transverse momentum distribution or quark-antiquark correlation observables (see *e.g.* Refs. [15, 16]).

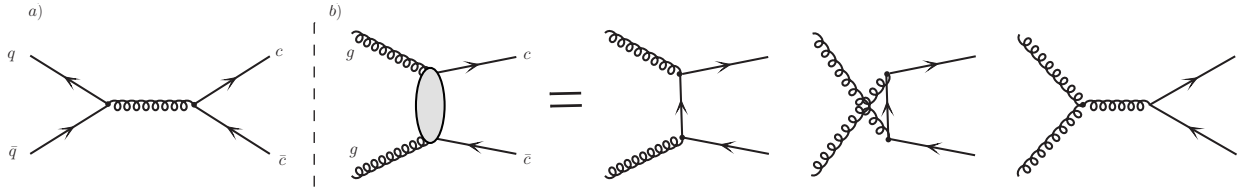


FIG. 1: Dominant mechanisms of charm quark production at leading-order: $q\bar{q}$ -annihilation (diagram a) and gg -fusion (diagrams b). These partonic processes lead to leading (standard) fragmentation component of D_s production.

The c and \bar{c} cross sections are calculated in the collinear NLO approximation using the FONLL framework [17] or in the k_t -factorization approach [18]. The latter calculations are done within both, the standard scheme with $2 \rightarrow 2$ hard subprocesses as well as within a new scheme with higher-order ($2 \rightarrow 3$ and $2 \rightarrow 4$) mechanisms included at the tree level¹

¹ We have checked numerically, that both prescriptions almost coincide for the KMR uPDF also at the rather low c.m.s. collision energy considered here.

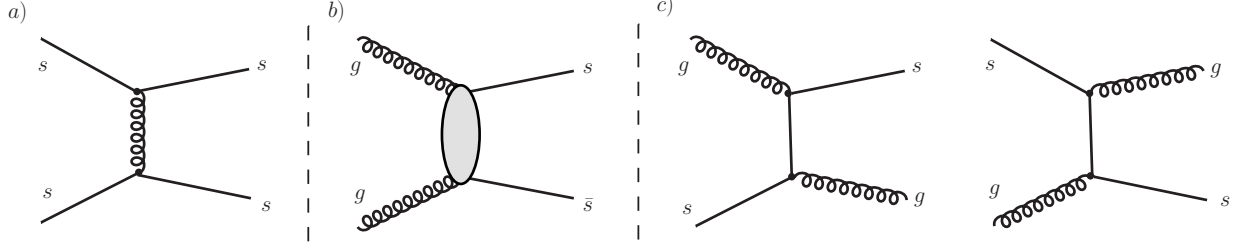


FIG. 2: An example of strange quark (or antiquark) production mechanisms at leading-order: $ss \rightarrow ss$ (diagram a), $gg \rightarrow s\bar{s}$ (diagram b), $gs \rightarrow gs$ and $sg \rightarrow sg$ (diagrams c). These partonic processes lead to subleading (unfavored) fragmentation component of D_s production.

[16]. Here, both the gg -fusion and $q\bar{q}$ -annihilation production mechanisms for $c\bar{c}$ -pairs with off-shell initial state partons are taken into consideration.

Not all charm hadrons must be created from the c/\bar{c} fragmentation. An extra hidden associated production of c and \bar{c} can occur in a complicated hadronization process. In principle, c and \bar{c} partons can also hadronize into light mesons (e.g. kaons) with non-negligible fragmentation fraction (see e.g. Ref. [19]). Similarly, fragmentation of light partons into heavy mesons may be well possible [20]. In the present study we will discuss also results of PYTHIA hadronization to D_s mesons in this context as well as our simple model of subleading fragmentation $s \rightarrow D_s^-$ and $\bar{s} \rightarrow D_s^+$ [13].

The s and \bar{s} distributions are calculated here in the leading-order (LO) collinear factorization approach with on-shell initial state partons and with a special treatment of minijets at low transverse momenta, as adopted e.g. in PYTHIA, by multiplying standard cross section by a somewhat arbitrary suppression factor [21]

$$F_{sup}(p_t) = \frac{p_t^4}{((p_t^0)^2 + p_t^2)^2}. \quad (2.1)$$

Within this framework the cross section of course strongly depends on the free parameter p_t^0 which could be, in principle, fitted to low energy charm experimental data [22]. Here, we use rather conservative value $p_t^0 = 1.5$ GeV. We use three different sets of the collinear parton distribution functions (PDFs): the MMHT2014 [23], the NNPDF30 [24] and the JR14NLO08FF [25] parametrizations. All of them provide an asymmetric strange sea quark distributions in the proton with $s(x) \neq \bar{s}(x)$. The dominant partonic mechanisms are $gs \rightarrow gs$, $g\bar{s} \rightarrow g\bar{s}$ (and their symmetric counterparts) and $gg \rightarrow s\bar{s}$. In some numerical calculations we take into account also other $2 \rightarrow 2$ diagrams with $s(\bar{s})$ -quarks in the final

state, however, their contributions are found to be almost negligible.

The transition from quarks to hadrons in our calculations is done within the independent parton fragmentation picture. Here, we follow the assumptions relevant for the case of low c.m.s. collision energies and/or small transverse momenta of hadrons, as discussed in our recent analysis [26], and we assume that the hadron H is emitted in the direction of parent quark/antiquark q , i.e. $\eta_H = \eta_q$ (the same pseudorapidities or polar angles). Within this approach we set the light-cone z -scaling, i.e. we define $p_H^+ = zp_q^+$, where $p^+ = E + p$. In the numerical calculations we also include “energy conservation” conditions: $E_H > m_H$ and $E_H \leq E_q$. If we take the parton as the only reservoir of energy (independent parton fragmentation) these conditions (especially the latter one) may be strongly broken in the standard fragmentation framework with constant rapidity $y_q = y_H$ scenario, especially, when discussing small transverse momenta of hadrons. The light-cone scaling prescription reproduces the standard approach in the limit: $m_q, m_H \rightarrow 0$.

For $c/\bar{c} \rightarrow D_s^\pm$ fragmentation we take the traditional Peterson fragmentation function with $\varepsilon = 0.05$. In contrast to the standard mechanism, the fragmentation function for $s/\bar{s} \rightarrow D_s^\mp$ transition is completely unknown which makes the situation more difficult. For the case of light-to-light (light parton to light meson) transition rather softer fragmentation functions (peaked at smaller z -values) are supported by phenomenological studies [27]. However, the light-to-heavy fragmentation should not be significantly different than for the heavy-to-heavy case. The shape of the fragmentation function depends on mass of the hadron rather than on the mass of parton (see e.g. Ref. [20]). Therefore, here we take the same fragmentation function for the $s/\bar{s} \rightarrow D_s^\mp$ as for the $c/\bar{c} \rightarrow D_s^\pm$. Besides the shape of the $s/\bar{s} \rightarrow D_s^\mp$ fragmentation function the relevant fragmentation fraction is also unknown. The transition probability $P = P_{s \rightarrow D_s}$ can be treated as a free parameter and needs to be extracted from experimental data. First attempt was done very recently in Ref. [13], where D_s^+/D_s^- production asymmetry was studied.

For further discussions in Table 1 we have collected total cross sections for different contributions to charm and strange quark production as well as to subsequent production of D_s^\pm mesons in proton-proton scattering at $\sqrt{s} = 27.4$ GeV. For the leading fragmentation mechanism here we compare results for $c\bar{c}$ -pair production calculated in the k_T -factorization approach and in the FONLL framework. The k_T -factorization approach leads to a slightly smaller cross sections than in the case of FONLL. At the rather low en-

TABLE I: Cross sections for charm and strangeness production in pp -collisions for $\sqrt{s} = 27.4$ GeV. For charm mesons $P_{c \rightarrow D_s} = 0.08$ and $P_{s \rightarrow D_s} = 0.05$ are used.

Framework/mechanism	Total cross section [μb]	
	partonic	D_s^+ or D_s^-
FONLL: all processes $\rightarrow c/\bar{c} \rightarrow D_s^+/D_s^-$		
MMHT2014nlo	12.568	0.510
CT14nlo	10.751	0.445
JR14NLO08FF	7.806	0.277
NNPDF30 NLO	4.955	0.200
k_T -fact. + KMR MMHT2014lo uPDF		
$g^*g^* \rightarrow c\bar{c}$ ($c/\bar{c} \rightarrow D_s^+/D_s^-$)	3.191	0.142
$q^*\bar{q}^* \rightarrow c\bar{c}$ ($c/\bar{c} \rightarrow D_s^+/D_s^-$)	0.164	0.007
k_T -fact. + KMR CT14lo uPDF		
$g^*g^* \rightarrow c\bar{c}$ ($c/\bar{c} \rightarrow D_s^+/D_s^-$)	4.642	0.241
$q^*\bar{q}^* \rightarrow c\bar{c}$ ($c/\bar{c} \rightarrow D_s^+/D_s^-$)	1.069	0.050
k_T -fact. + PB-NLO-set1 uPDF		
$g^*g^* \rightarrow c\bar{c}$ ($c/\bar{c} \rightarrow D_s^+/D_s^-$)	2.254	0.073
$q^*\bar{q}^* \rightarrow c\bar{c}$ ($c/\bar{c} \rightarrow D_s^+/D_s^-$)	1.286	0.055
LO coll. + MMHT2014lo PDF		
$gg \rightarrow s\bar{s}$ ($s/\bar{s} \rightarrow D_s^-/D_s^+$)	1.603	0.032
$is \rightarrow is + si \rightarrow si$ ($s \rightarrow D_s^-$)	4.789×2	0.149
$i\bar{s} \rightarrow i\bar{s} + \bar{s}i \rightarrow \bar{s}i$ ($\bar{s} \rightarrow D_s^+$)	3.769×2	0.098
LO coll. + NNPDF30 LO PDF		
$gg \rightarrow s\bar{s}$ ($s/\bar{s} \rightarrow D_s^-/D_s^+$)	0.947	0.016
$is \rightarrow is + si \rightarrow si$ ($s \rightarrow D_s^-$)	1.960×2	0.114
$i\bar{s} \rightarrow i\bar{s} + \bar{s}i \rightarrow \bar{s}i$ ($\bar{s} \rightarrow D_s^+$)	0.988×2	0.047
LO coll. + JR14NLO08FF PDF		
$gg \rightarrow s\bar{s}$ ($s/\bar{s} \rightarrow D_s^-/D_s^+$)	0.733	0.010
$is \rightarrow is + si \rightarrow si$ ($s \rightarrow D_s^-$)	2.616×2	0.086
$i\bar{s} \rightarrow i\bar{s} + \bar{s}i \rightarrow \bar{s}i$ ($\bar{s} \rightarrow D_s^+$)	2.413×2	0.082

ergy considered here the dominant production mechanism is still the gg -fusion, however, the $q\bar{q}$ -annihilation is found to be also important. This statement is true for calculations with both, on-shell and off-shell partons. For the calculations with off-shell partons we

use three different sets of uPDFs: two sets of the Kimber-Martin-Ryskin (KMR) model [28] based on MMHT2014lo [23] and CT14lo [29] collinear PDFs and one set of parton-branching model PB-NLO-set1 [30]. In general, several uPDFs lead to a quite similar results, especially for $g^*g^* \rightarrow c\bar{c}$ mechanism. In the case of $q^*\bar{q}^* \rightarrow c\bar{c}$ channel results of the KMR-CT14lo and PB-NLO-set1 almost coincide, however, we found a significant difference between these two results and the result obtained with the KMR-MMHT2014lo. The discrepancy between KMR-CT14lo and KMR-MMHT2014lo results comes from a significant differences of up and down quark distributions at very small- Q^2 and large- x incorporated in the MMHT2014lo and CT14lo collinear PDFs². The major part of the cross section for $q^*\bar{q}^* \rightarrow c\bar{c}$ mechanism at $\sqrt{s} = 27.4$ GeV comes from the $x \approx 10^{-1}$ and $k_t \approx 1$ GeV kinematical regime. In the KMR procedure, transverse momentum of the incoming parton k_t plays a role of the scale Q in the collinear PDF which is an input for the calculation of the uPDF. In fact, for calculations with the KMR uPDFs here, one is very sensitive to the rather poorly constrained region of the collinear PDFs.

Switching to collinear approximation, we do not approach these problematic regions since the lower limit of the factorization scale is then set to be equal to the charm quark mass, so the minimal scale is $Q_{\min}^2 = 2.25 \text{ GeV}^2$. For the FONLL predictions different collinear PDFs were used. Various PDF parametrizations lead to very different results. The total cross sections are very sensitive to the low- p_t region which is very uncertain at this low energy. The predicted cross sections strongly depend on the low- Q^2 parametrizations of the collinear PDFs which are not under full theoretical control. This uncertainty may be crucial for the further predictions of neutrino production at the SHiP experiment which, as will be shown in the next sections, is mostly driven by this problematic kinematical region. As already mentioned, the situation may be even more complicated in the case of the k_T -factorization approach where less-known objects, i.e. transverse-momentum-dependent uPDFs, are used. Besides the PDF uncertainties, at very low charm quark transverse momenta FONLL predictions (in general any pQCD calculations) are very sensitive to the choice of the renormalization/factorization scale and the charm quark mass (see e.g. Ref. [15]). These uncertainties may be crucial especially in the case

² For gluon and strange quark production both models provide rather similar distributions, the differences are much smaller than in the case of up and down quarks.

TABLE II: Number of D_s mesons per 10^6 generations of hard processes, fraction of a given mechanism and respective cross sections in nanobarns from PYTHIA Monte Carlo generator. Here we collected numbers for $D_s^+ + D_s^-$ mesons.

PYTHIA: 10^6 generations	$N(D_s^+) + N(D_s^-)$	fraction [%]	cross section [nb]
total	1467+1771	100.0	1156
$gg \rightarrow c\bar{c}$	1099	33.9	392
$q\bar{q} \rightarrow c\bar{c}$	163	5.0	58
$gg \rightarrow gg$	174	5.4	62
$q/\bar{q}g$	1088	33.6	388
qq' , etc.	713	22.0	255

of charm flavour production at low energies but were discussed many times in the literature.

For strange quark and/or antiquark production we consider all the dominant partonic $2 \rightarrow 2$ processes. Here we show separately results for gg -fusion and for other mechanisms with s or \bar{s} quark or antiquark in the initial and final state, denoted as $is \rightarrow is$ or $i\bar{s} \rightarrow i\bar{s}$ where $i = u, d, s, g, \bar{u}, \bar{d}, \bar{s}$. The cross sections for strange quark/antiquark production are of the same order of magnitude as in the case of charm production. According to the obtained partonic cross sections, both fragmentation mechanisms - leading and subleading, are predicted to contribute to the D_s^\pm -meson cross section at the similar level. Also here, we show results for different collinear PDFs. We have intentionally chosen the PDF parametrizations that lead to an asymmetry in production of s and \bar{s} . Within these models the s -quarks are produced more frequently than the \bar{s} -antiquarks and the largest production asymmetry is obtained for the NNPDF30 PDF.

The overall picture for D_s^\pm -meson production based on the independent parton fragmentation framework with leading and subleading fragmentation components seem to be similar to the picture present in the PYTHIA Monte Carlo generator. In Table II we show the number of D_s^\pm mesons per 10^6 generations of hard processes, fraction of a given mechanism and respective cross sections in nanobarns obtained from the PYTHIA generator. The partonic structure of the D_s^\pm meson production in PYTHIA is rather similar to the structure obtained in our model. The dominant mechanisms here are $gg \rightarrow c\bar{c}$ (our

leading component) and $q(\bar{q})g \rightarrow q(\bar{q})g$ and $qq' \rightarrow qq'$ (our subleading components). Both models lead to a very similar results for the leading component. For the subleading contributions, our model slightly underestimates the PYTHIA predictions. Also here we got a clear production asymmetry $N(D_s^+) = 1467$ and $N(D_s^-) = 1771$, which is important in the context of the production asymmetry of neutrinos/antineutrinos.

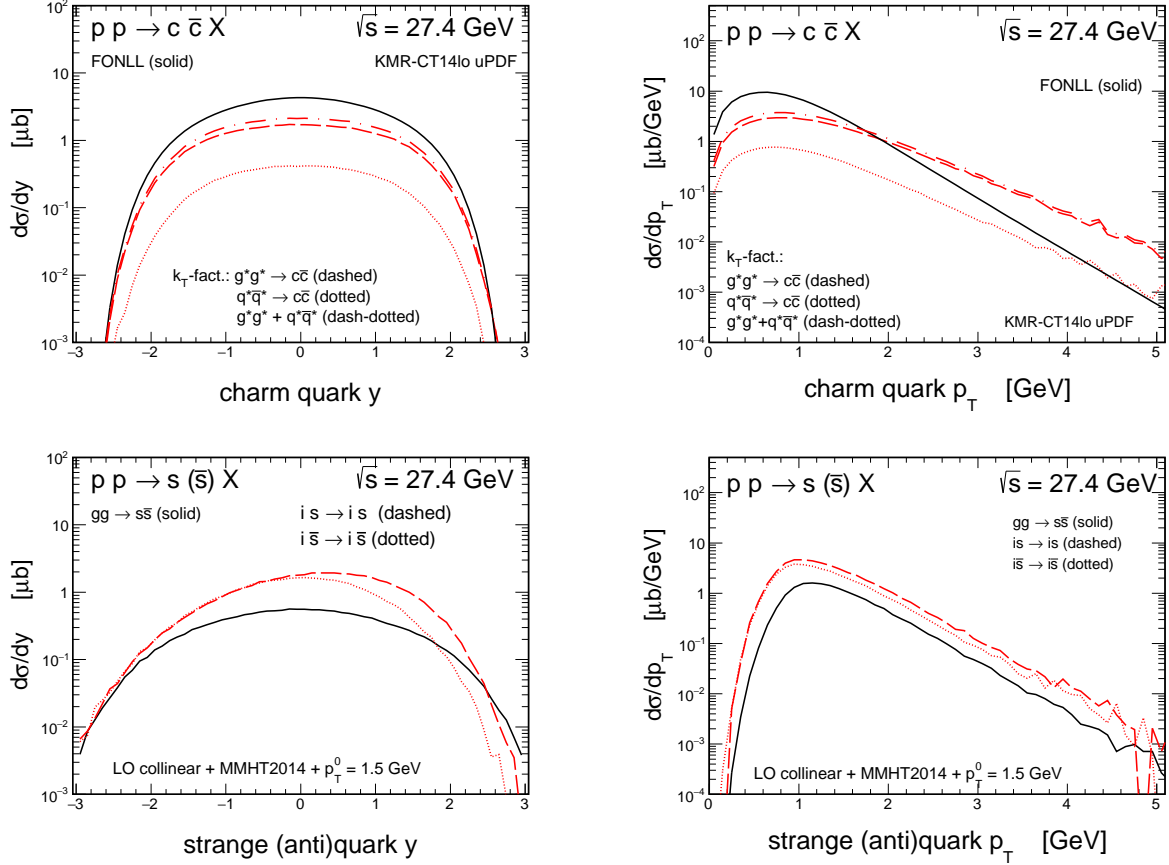


FIG. 3: Rapidity (left) and transverse momentum (right) distributions of charm (top) and strange (bottom) quarks. Contributions of different mechanisms are shown separately. For strange quarks only contributions of $is \rightarrow is$ or $i\bar{s} \rightarrow i\bar{s}$ ($i = g, q, \bar{q}$) are shown. Similar contributions for $si \rightarrow si$ or $\bar{s}i \rightarrow \bar{s}i$ can be obtained by the $y \rightarrow -y$ symmetry operation. Other details are specified in the figure.

In Fig. 3 we compare distributions of c/\bar{c} and s/\bar{s} quarks/antiquarks (top and bottom panels) produced in proton-proton collisions at $\sqrt{s} = 27.4$ GeV. For charm quarks we get a very similar rapidity distributions within both the FONLL (solid lines) and the k_T -factorization (dash-dotted lines) frameworks. For the latter case we show separately g^*g^*

(dashed lines) and $q^*\bar{q}^*$ (dotted lines) components. For the quark transverse momentum distribution we obtain some differences between both approaches. At very small transverse momenta the FONLL code leads to a larger cross section than that obtained in the k_T -factorization. However, at larger p_T 's the situation reverses and the k_T -factorization result now become larger. This may be a combined result of several effects, *i.e.* the effect of keeping exact kinematics from the very beginning in the k_T -factorization, the effect of the off-shellness of the incident partons and in some limited amount also the effect of the beyond NLO contributions effectively included at the tree-level in the k_T -factorization approach [16] which are missing in the FONLL framework.

In general, the cross section for s/\bar{s} quarks/antiquarks are of similar order of magnitude as that for $c\bar{c}$ production (see top and bottom panels of Fig. 3). For strange quarks we show separately the two dominant channels (or classes of channels): gg -fusion (solid lines) and $is \rightarrow is$ or $i\bar{s} \rightarrow i\bar{s}$ (dashed and dotted lines). For the latter mechanisms we obtain a clear asymmetry between production of s -quark and \bar{s} -antiquark which is a direct consequence of the $s(x) \neq \bar{s}(x)$ asymmetry in the MMHT2014lo PDFs.

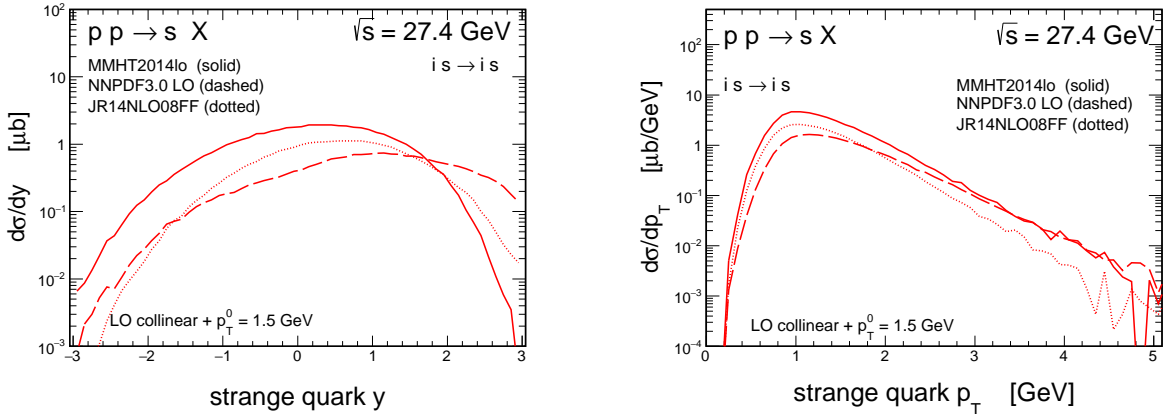


FIG. 4: Rapidity (left) and transverse momentum (right) distributions of strange quarks from $is \rightarrow is$ mechanisms for different sets of collinear PDFs. Details are specified in the figure.

Of course, different PDFs may lead to a different distributions of s -quark and \bar{s} -antiquark and also to different size of their production asymmetry. In Fig. 4 we present rapidity (left panel) and transverse momentum (right panel) distributions of s -quark from the $is \rightarrow is$ class of processes for different PDFs from the literature. Quite different rapidity distributions are obtained from the different PDFs, especially in the (very)forward region where the differences are really large. In the consequence this will generate uncer-

tainties for far-forward (very large rapidities) production of D_s meson and $\nu_\tau/\bar{\nu}_\tau$ neutrinos/antineutrinos as well.

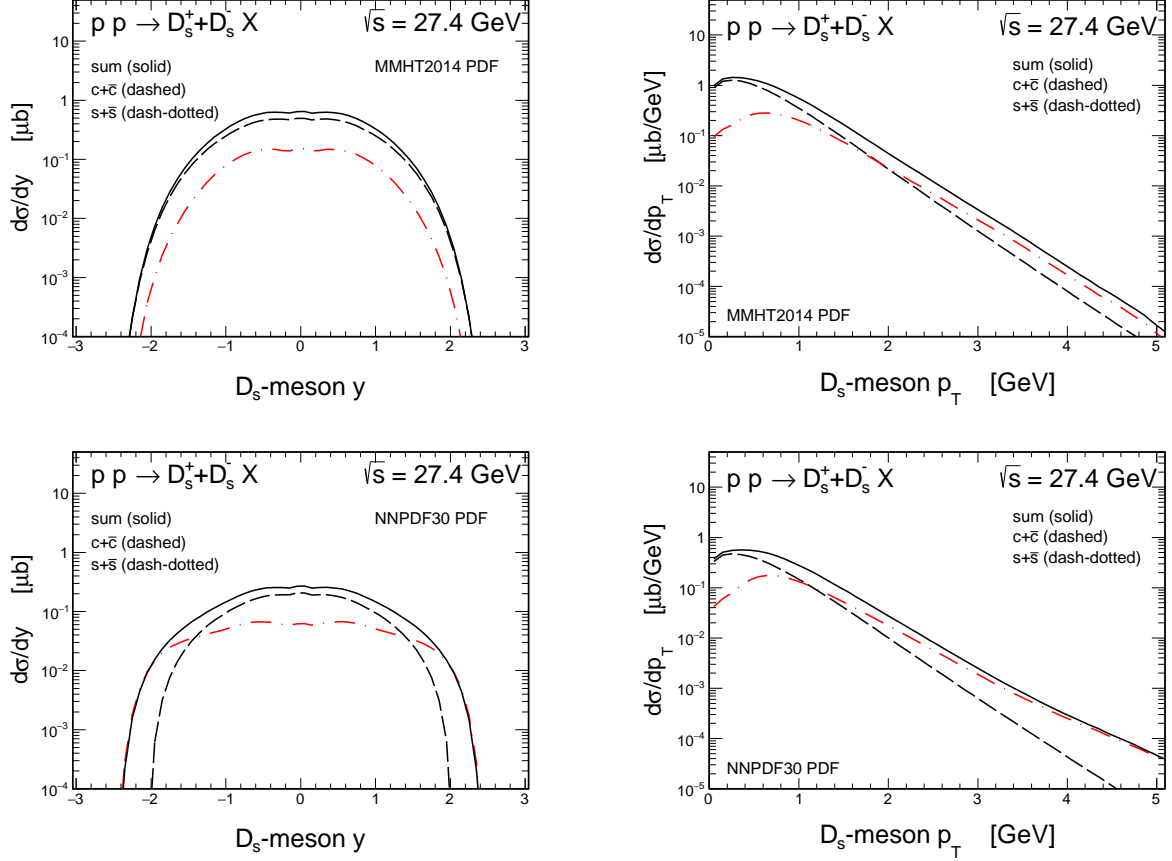


FIG. 5: Rapidity (left) and transverse momentum (right) distributions of D_s mesons for the MMHT2014 (top) and NNPDF30 (bottom) sets of collinear PDFs. Contributions from charm and strange quark fragmentation are shown separately. Details are specified in the figure.

In Fig. 5 we show the resulting rapidity (left panel) and transverse momentum (right panel) distributions of D_s mesons from proton-proton scattering at $\sqrt{s} = 27.4$ GeV. We compare contributions of the leading ($c/\bar{c} \rightarrow D_s^\pm$) and the subleading ($s/\bar{s} \rightarrow D_s^\mp$) mechanisms, calculated in the FONLL and in the LO collinear approach, respectively. In this calculation $P_{c \rightarrow D_s} = 0.08$ and $P_{s \rightarrow D_s} = 0.05$ were used. Top and bottom panels show results for different collinear PDF sets from the literature. While for the MMHT2014 PDF the subleading contribution is always smaller than the leading one, for the NNPDF30 PDF it is not the case and the subleading contribution wins above $|y| > 2$. The subleading contribution also wins at larger meson transverse momenta and changes the slope

of the distribution in a visible way. Again the effect is stronger for the calculations with the NNPDF30 PDF which leads to a smaller leading contribution than in the case of the MMHT2014 PDF. This demonstrates uncertainties related to the production mechanism. Related consequences for the production of $\nu_\tau/\bar{\nu}_\tau$ will be discussed in section III B.

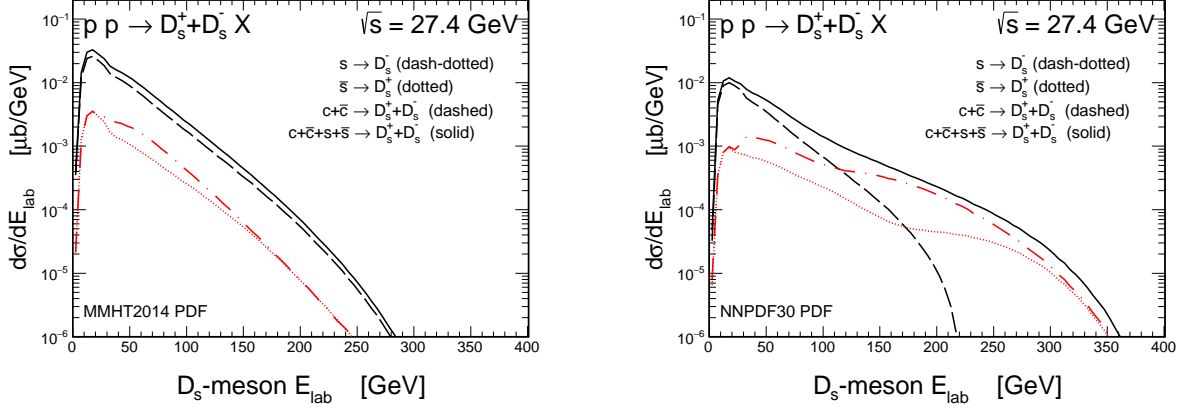


FIG. 6: Energy distributions of D_s mesons in the laboratory frame for the MMHT2014 (left) and the NNPDF30 (right) sets of collinear PDFs. Contributions from charm and strange quark fragmentation are shown separately. Details are specified in the figure.

Finally, in Fig. 6, we show how these PDF uncertainties discussed above affect predictions for the energy distribution of D_s mesons in the laboratory frame. Here we show separately the leading $c + \bar{c} \rightarrow D_s^+ + D_s^-$ (dashed lines) and two subleading $s \rightarrow D_s^-$ (dash-dotted lines) and $\bar{s} \rightarrow D_s^+$ (dotted lines) contributions as well as their sum $c + \bar{c} + s + \bar{s} \rightarrow D_s^+ + D_s^-$ (solid lines). The left and right panels correspond to the MMHT2014 and the NNPDF30 PDFs, respectively. Again a pretty much different results are obtained for the two different PDF sets, especially for large meson energies. Depending on the collinear PDFs used our model leads to a rather small (the MMHT2014 PDF) or a fairly significant (the NNPDF30 PDF) contribution to the D_s meson production at large energies which comes from the s/\bar{s} -quark fragmentation.

Summarizing this part we see big uncertainties in our predictions for the production of D_s mesons at the low $\sqrt{s} = 27.4$ GeV energy. A future measurement of D_s mesons at low energies would definitely help to better understand underlying mechanism and in the consequence improve predictions for $\nu_\tau/\bar{\nu}_\tau$ production for the SHiP experiment.

B. Direct decay of D_s^\pm mesons

The considered here decay channels: $D_s^+ \rightarrow \tau^+ \nu_\tau$ and $D_s^- \rightarrow \tau^- \bar{\nu}_\tau$, which are the sources of the direct neutrinos, are analogous to the standard text book cases of $\pi^+ \rightarrow \mu^+ \nu_\mu$ and $\pi^- \rightarrow \mu^- \bar{\nu}_\mu$ decays, discussed in detail in the past (see e.g. Ref [31]). The same formalism used for the pion decay applies also to the D_s meson decays. Since pion has spin zero it decays isotropically in its rest frame. However, the produced muons are polarized in its direction of motion which is due to the structure of weak interaction in the Standard Model. The same is true for D_s^\pm decays and polarization of τ^\pm leptons.

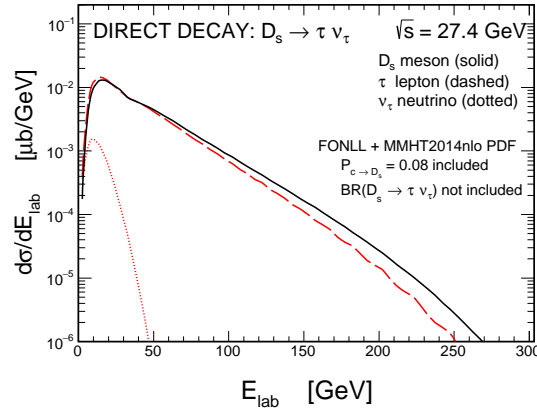


FIG. 7: Laboratory energy distributions of D_s mesons (solid), τ leptons (dashed) and ν_τ neutrinos (dotted) from the direct decay $D_s \rightarrow \tau \nu_\tau$. Here we show only the leading contribution to D_s meson production from charm quarks calculated with the FONLL code. The decay branching fraction is not included here for easier comparison.

Therefore the τ decay must be carefully considered. In such decays the τ particles are strongly polarized with $P_{\tau^+} = -P_{\tau^-}$. In the following we assume that in the rest frame of D_s meson:

$$P_{\tau^-} = 1 \text{ and } P_{\tau^+} = -1 \quad .$$

This is also very good approximation in the rest frame of τ^\pm .

To calculate cross section for $\nu_\tau/\bar{\nu}_\tau$ production the $D_s^\pm \rightarrow \tau^\pm \nu_\tau/\bar{\nu}_\tau$ branching fraction must be included. The decay branching fraction is rather well known: $\text{BR}(D_s^\pm \rightarrow \tau^\pm \nu_\tau/\bar{\nu}_\tau) = 0.0548 \pm 0.0023$ [9].

In Fig. 7 we show laboratory frame energy distribution of D_s meson (solid line) and τ lepton (dashed line) and ν_τ neutrino (dotted line) from the direct decay. It can be clearly seen that the τ lepton takes almost whole energy of the mother D_s meson.

C. Neutrinos from chain decay of τ leptons

The τ decays are rather complicated due to having many possible decay channels [9]. Nevertheless, all confirmed decays lead to production of ν_τ ($\bar{\nu}_\tau$). This means total amount of neutrinos/antineutrinos produced from D_s decays into τ lepton is equal to the amount of antineutrinos/neutrinos produced in subsequent τ decay. But, their energy distributions will be different due to D_s production asymmetry in the case of the subleading fragmentation mechanism.

The purely leptonic channels (three-body decays), analogous to the $\mu^\pm \rightarrow e^\pm(\bar{\nu}_\mu/\nu_\mu)(\nu_e/\bar{\nu}_e)$ decay (discussed e.g. in Refs. [31, 33]) cover only about 35% of all τ lepton decays. Remaining 65% are semi-leptonic decays. They differ quite drastically from each other and each gives slightly different energy distribution for ν_τ ($\bar{\nu}_\tau$). In our model for the decay of D_s mesons there is almost full polarization of τ particles with respect to the direction of their motion.

Since $P_{\tau^+} = -P_{\tau^-}$ (see the previous subsection) and the angular distributions of polarized τ^\pm are antisymmetric with respect to the spin axis the resulting distributions of ν_τ and $\bar{\nu}_\tau$ from decays of D_s^\pm are then identical, consistent with CP symmetry (see e.g. Ref. [32]).

The mass of the τ lepton (1.777 GeV) is very similar as the mass of the D_s meson (1.968 GeV). Therefore, direct neutrino takes away only a small fraction of energy/momentum of the mother D_s . In this approximation:

$$\vec{v}_\tau = \vec{v}_{D_s}, \quad \vec{p}_\tau = \vec{p}_{D_s} \quad (2.2)$$

polarization of τ in its rest frame is 100 %. In reality polarization of τ^\pm is somewhat smaller. In the approximate Z-moment method often used for production of neutrinos/antineutrinos in the atmosphere discussed e.g. in Ref. [33] the polarization is a function of E_τ/E_{D_s} (see also Ref. [34]).

Before we go to distribution of neutrinos/antineutrinos in the laboratory system (fixed

target $p + {}^{96}\text{Mo}$ collisions) we shall present distributions of neutrinos/antineutrinos in the τ^\pm center-of-mass system, separately for different decay channels of τ . In this calculation we use TAUOLA code [35].

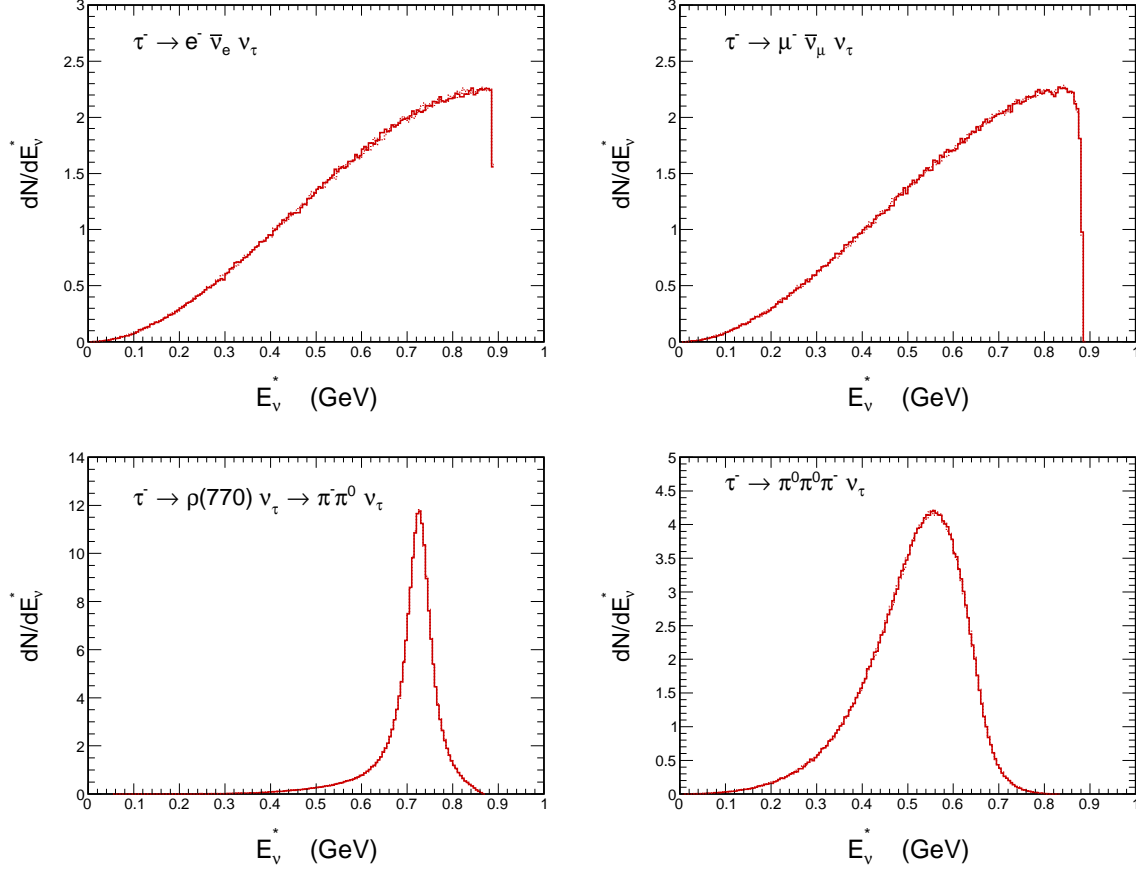


FIG. 8: Distributions in energy of ν_τ in the τ^- center-of-mass system, for selected decay channels. The counterpart distributions for $\bar{\nu}_\tau$ from the decay of τ^+ are identical. Note that, top plots, which are quite similar, cover about 35% of all tau decays. Therefore, dominant contribution comes from semi-leptonic decays, which lead to rather different distributions.

In Fig. 8 we show distribution in energy E^* of neutrinos in the τ center-of-mass system, for selected decay channels. Quite different distributions are obtained for different decay channels. In Fig. 9 we show distributions in $z^* = \cos(\theta^*)$ of the neutrinos with respect to τ spin direction, again separately for different decay channels. The distribution functions are linear in z^* which could simplify calculations.

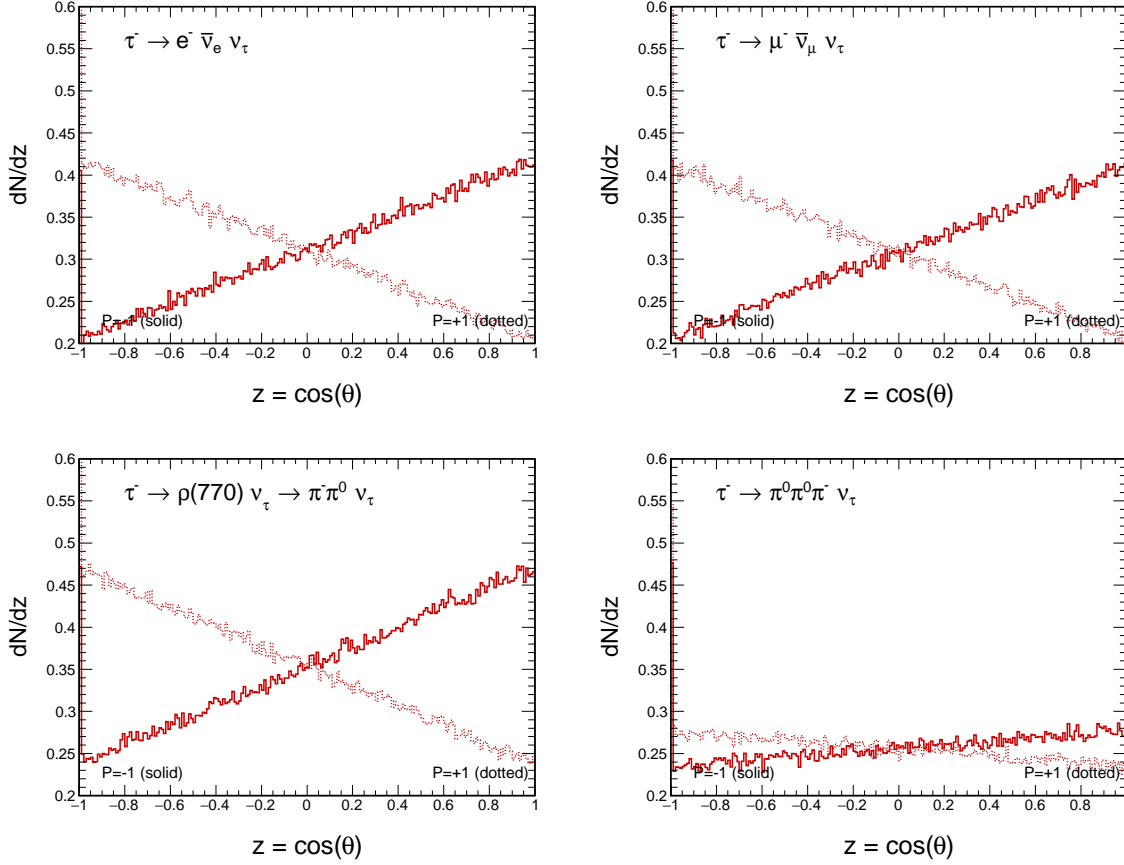


FIG. 9: Distributions in $z^* = \cos(\theta^*)$ of ν_τ in the τ^- center-of-mass system for two polarizations of τ^- particles ($P = \pm 1$). For charged conjugate channels with $\bar{\nu}_\tau$ the distributions must be symmetrically inverted $P(\tau^-) = \pm 1 \rightarrow P(\tau^+) = \mp 1$.

D. $p + {}^{96}\text{Mo}$ collisions

The differential cross section $d\sigma/dydp_t$ for D_s^\pm production in $p + {}^{96}\text{Mo}$ collision is assumed to approximately scale like

$$\frac{d\sigma_{p+\text{Mo}}}{dydp_t} = Z_{\text{Mo}} \frac{d\sigma_{pp}}{dydp_t} + (A_{\text{Mo}} - Z_{\text{Mo}}) \frac{d\sigma_{pn}}{dydp_t}. \quad (2.3)$$

It was shown in [36] that at much higher energies ($\sqrt{s}_{NN} = 5.02$ GeV) the nuclear modification factor for D meson production in $p + \text{Pb}$ is close to 1 in a broad range of rapidity and transverse momentum. This is an approximation which is not easy to improve in a realistic way. Therefore it is difficult at present to set uncertainties of such an approximation. In our calculation collision energy was fixed $\sqrt{s}_{NN} = 27.4$ GeV. For more precise calculation one has to consider calculating a cascade which was attempted e.g. in [38].

E. Neutrino/antineutrino interactions with the Pb target

How many neutrinos/antineutrinos will be observed in the SHiP experiment depends on the cross section for neutrino/antineutrino scattering of nuclei off the target. In the case of the SHiP experiment a dedicated lead target was proposed. At not too small energies ($\sqrt{s_{NN}} > 5$ GeV), the cross section for $\nu_\tau Pb$ and $\bar{\nu}_\tau Pb$ interactions can be obtained from elementary cross sections as:

$$\sigma(\nu_\tau Pb) = Z\sigma(\nu_\tau p) + (A - Z)\sigma(\nu_\tau n) , \quad (2.4)$$

$$\sigma(\bar{\nu}_\tau Pb) = Z\sigma(\bar{\nu}_\tau p) + (A - Z)\sigma(\bar{\nu}_\tau n) . \quad (2.5)$$

Shadowing effects depend on x variable (parton longitudinal momentum fraction), i.e. on neutrino/antineutrino energy. At not too high energies (not too small x) shadowing effects are rather small and can be neglected at present accuracy having in mind other uncertainties. On the other hand for the x -ranges considered here the antishadowing and/or EMC-effect may appear non-negligible but still rather small and shall not affect the numerical predictions presented here. The nuclear modifications of the PDFs goes beyond the scope of the present study and will be considered elsewhere.

Both elementary as well as nuclear cross sections strongly depend on neutrino/antineutrino energy [14]. For τ neutrino/antineutrino interactions there is also an energy threshold related to the mass of τ^\pm which reduces cross section compared to $\nu_\mu/\bar{\nu}_\mu$ and practically cuts off contributions of nucleon resonances. Therefore one should include practically only deep-inelastic region.

The probability of interacting of neutrino/antineutrino with the lead target can be calculated as:

$$P_{\nu_\tau/\bar{\nu}_\tau}^{\text{target}}(E) = \int_0^d n_{\text{cen}} \sigma_{\nu_\tau Pb}(E) dz = n_{\text{cen}} \sigma_{\nu_\tau Pb}(E) d , \quad (2.6)$$

where n_{cen} is a number of scattering centers (lead nuclei) per volume element and the target thickness is $d \approx 2$ m [7]. Using the NUWRO Monte Carlo generator [37], we obtain $\sigma(E)/E \sim 1.09 \times 10^{-38}$ cm²/GeV for neutrino and 0.41×10^{-38} cm²/GeV for antineutrino for the $E = 100$ GeV. The number of scattering centers is

$$n_{\text{cen}} = (11.340/207.2)N_A , \quad (2.7)$$

where $N_A = 6.02 \times 10^{23}$ is the Avogadro number.

The energy dependent flux of neutrinos can be written as:

$$\Phi_{\nu_\tau/\bar{\nu}_\tau}(E) = \frac{N_p}{\sigma_{pA}} d\sigma_{pA \rightarrow \nu_\tau}(E)/dE, \quad (2.8)$$

where N_p is integrated number of beam protons ($N_p = 2 \times 10^{20}$ according to the current SHiP project). The σ_{pA} in Eq. (2.8) is a crucial quantity which requires a short discussion. In Ref. [8] it was taken as $\sigma_{pA} = A \cdot \sigma_{pN}$ where $\sigma_{pN} = 10.7$ was used. We do not know the origin of this number. Naively σ_{pN} should be the inelastic pN cross section.

The formula above can be used to estimate number of neutrinos/antineutrinos produced at the beam dump. For the decays of D_s meson produced from charm quark fragmentation it reads:

$$N_{\nu_\tau} = \frac{N_p}{\sigma_{pA}} \sigma_{pA \rightarrow \nu_\tau X} = \frac{N_p}{\sigma_{pN}} \sigma_{pp \rightarrow c\bar{c}} \text{BR}(D_s \rightarrow \tau) P(c \rightarrow D_s). \quad (2.9)$$

Taking $P(c \rightarrow D_s) = 0.08$, $\text{BR}(D_s \rightarrow \tau) = 0.0548$, $\sigma_{pp \rightarrow c\bar{c}X} = 10 \mu\text{b}$ and $\sigma_{pN} = 20 \text{ mb}$ we get $N_{\nu_\tau} = 0.66 \times 10^{15}$. Already this number is rather uncertain mostly due to the choice of σ_{pA} and $pp \rightarrow c\bar{c}$ cross section. This is almost an order of magnitude lower than the corresponding number(s) in Table 2 of Ref. [7]. The numbers presented there and the reason of the discrepancy are not clear for us.

In the present paper the elementary cross sections $\sigma(\nu_\tau p)$, $\sigma(\nu_\tau n)$, $\sigma(\bar{\nu}_\tau p)$ and $\sigma(\bar{\nu}_\tau n)$ needed in Eq.(2.5) are calculated using the NUWRO Monte Carlo generator. In Fig. 10 we show the cross section for scattering neutrinos/antineutrinos on the protons and neutrons (left panel) and on the lead target (right panel) as a function of neutrino/antineutrino energy. The cross sections at larger energies are fully dominated by the charged current deep-inelastic scattering interactions (more than 90% of the cross section for $E_\nu \geq 15 \text{ GeV}$). In the left panel we observe that all the cross sections strongly depend on neutrino energy. While for the proton target the cross section for neutrino and antineutrino is almost the same, for the neutron target they are quite different. In the right panel we show the cross sections $\sigma(\nu_\tau \text{Pb})$ and $\sigma(\bar{\nu}_\tau \text{Pb})$. Here we take only the dominant isotope ^{208}Pb . Isotope admixture of ^{204}Pb , ^{206}Pb , ^{207}Pb in the target for neutrino/antineutrino observation makes only small corrections which is of academic value only. We show separately results obtained by the elementary cross sections using Eq.(2.5) (dashed lines) and those obtained directly for the lead target³ including

³ obtained within the local Fermi gas model for the description of the nucleus as a target

some nuclear effects (solid lines). For our purpose the difference between the two results is rather marginal. The cross sections will be used to estimate the number of neutrino/antineutrino observations.

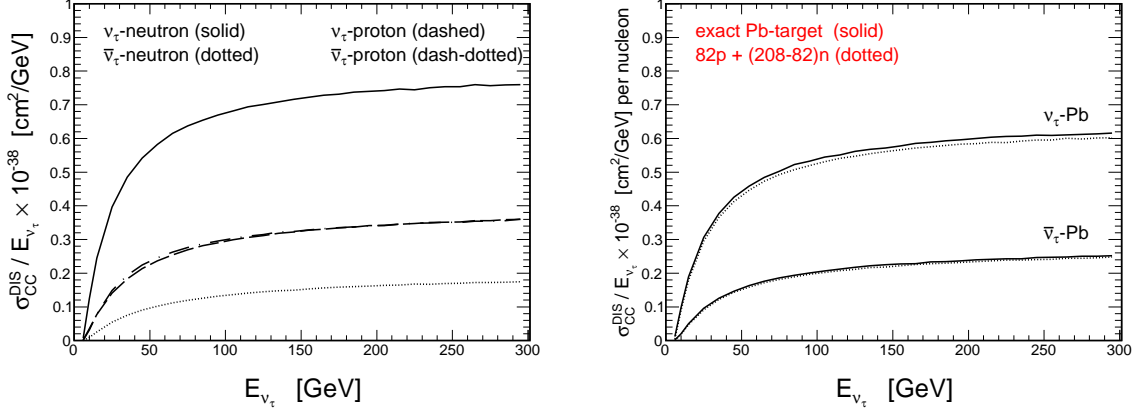


FIG. 10: Left: The elementary cross sections $\sigma(\nu_\tau p)$, $\sigma(\nu_\tau n)$, $\sigma(\bar{\nu}_\tau p)$ and $\sigma(\bar{\nu}_\tau n)$ as a function of neutrino/antineutrino energy. Right: The $\sigma(\nu_\tau \text{Pb})$ and $\sigma(\bar{\nu}_\tau \text{Pb})$ cross sections per nucleon as a function of neutrino/antineutrino energy. The results are obtained within the NUWRO Monte Carlo generator. Details are specified in the figure.

Finally the number of neutrinos/antineutrinos observed in the *Pb* target is calculated from the formula:

$$N_{\nu_\tau/\bar{\nu}_\tau}^{\text{target}} = \int dE \Phi_{\nu_\tau/\bar{\nu}_\tau}(E) P_{\nu_\tau/\bar{\nu}_\tau}^{\text{target}}(E). \quad (2.10)$$

Here $\Phi_{\nu_\tau/\bar{\nu}_\tau}(E)$ is calculated from different approaches to D_s meson production including their subsequent decays and $P_{\nu_\tau/\bar{\nu}_\tau}^{\text{target}}(E)$ is obtained using Eq.(2.6). The cross sections for neutrino/antineutrino interactions with the lead target is shown in Fig. 10.

III. NUMERICAL PREDICTIONS FOR THE SHIP EXPERIMENT

A. Neutrino/antineutrino differential cross sections for $p + {}^{96}\text{Mo}$ at $\sqrt{s_{NN}} = 27.4$ GeV

We start presentation of our numerical results with the differential cross sections for ν_τ or $\bar{\nu}_\tau$ neutrino production. In Fig. 11 we show transverse momentum distributions of neutrinos/antineutrinos for $p + {}^{96}\text{Mo}$ interactions at $\sqrt{s_{NN}} = 27.4$ GeV with the $\eta_\nu > 5.3$ condition relevant for the SHiP experiment. The predictions are done for both the leading (left panels) and for the subleading (right panels) D_s -meson production mechanisms

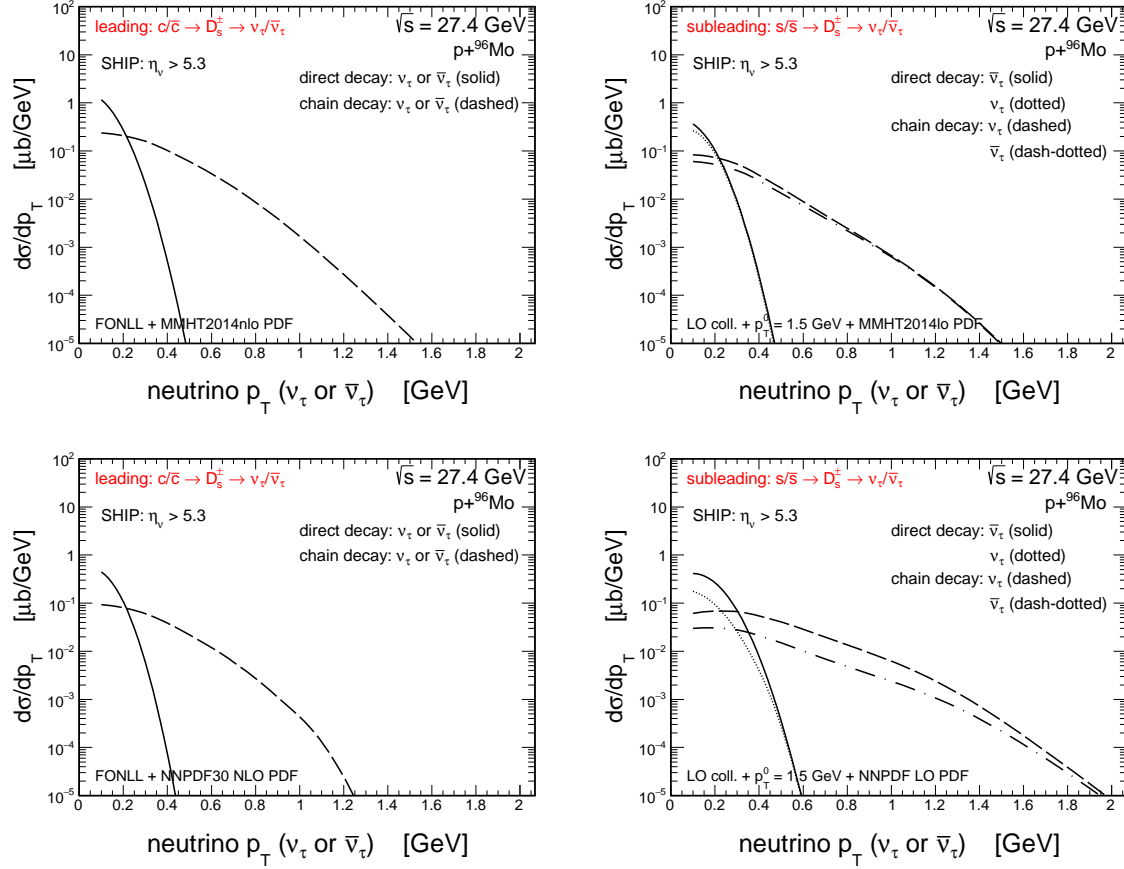


FIG. 11: Transverse momentum distributions of ν_τ (or $\bar{\nu}_\tau$) neutrinos for the MMHT2014 (top) and the NNPDF30 (bottom) sets of collinear PDFs for the leading (left) and subleading (right) D_s -meson production mechanisms. Contributions from the direct and chain decay modes are shown separately. Further details are specified in the figure.

calculated with the MMHT2014 (top panels) and the NNPDF30 (bottom panels) PDFs. Here, we show separately distributions for ν_τ and $\bar{\nu}_\tau$ from the direct and chain decay modes. The direct contributions are concentrated in the region of extremely small transverse momenta while their chain counterparts have significantly longer tails in p_T . Even for the chain decays the major parts of the cross sections come from the region of small transverse momentum ($p_T < 2$ GeV) of neutrino. The contributions for the subleading $s/\bar{s} \rightarrow D_s^\pm$ show a visible production asymmetry for ν_τ and $\bar{\nu}_\tau$ in contrast to the contributions for the standard leading $c/\bar{c} \rightarrow D_s^\pm$ mechanism. The $s(x) \neq \bar{s}(x)$ asymmetry in the parton distributions leads to the neutrino/antineutrino production asymmetry for both, the direct and the chain decay modes. The obtained cross sections for s -quark production

are larger than those for the \bar{s} -antiquark. For the direct decay mode this leads to enhanced production of $\bar{\nu}_\tau$ antineutrinos with respect to the ν_τ neutrinos. The effect is opposite in the case of the chain decay mode where $s \rightarrow \nu_\tau$ and $\bar{s} \rightarrow \bar{\nu}_\tau$. The production asymmetry is larger when the NNPDF30 PDFs are used than in the case of the MMHT2014 PDFs.

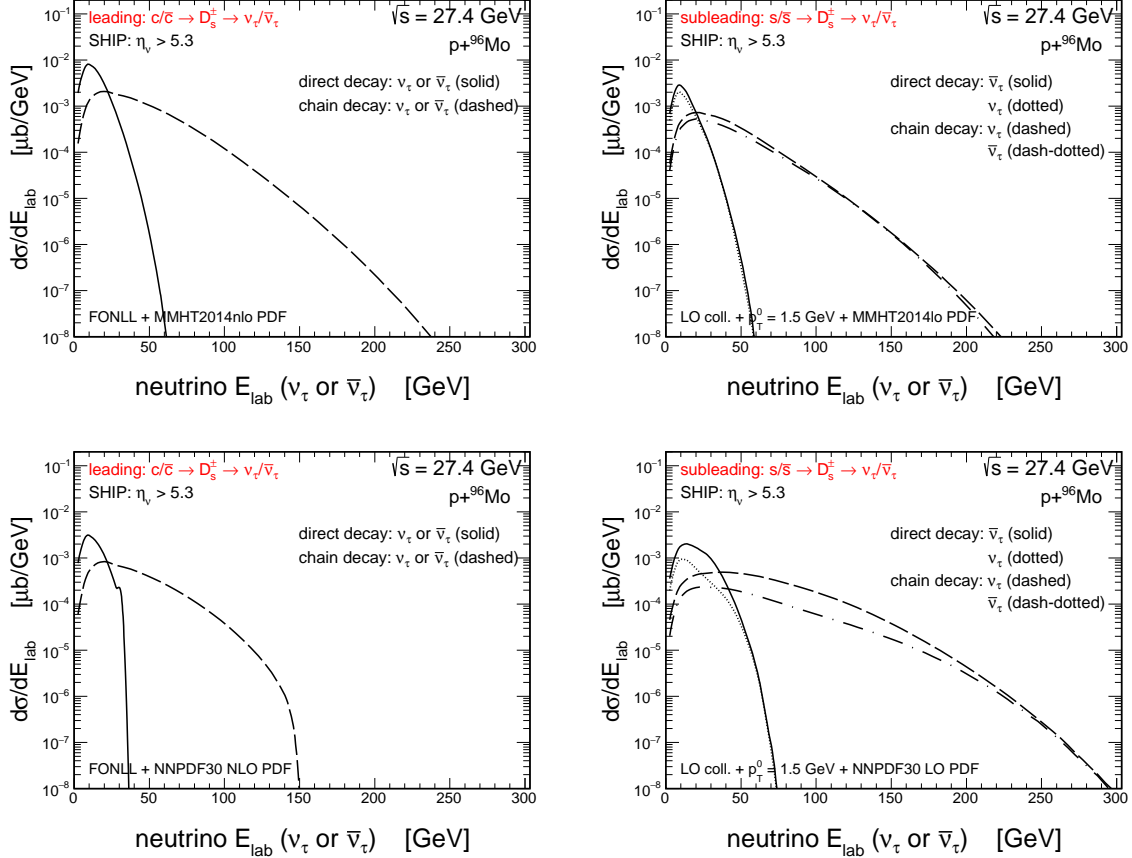


FIG. 12: Laboratory frame energy distributions of ν_τ (or $\bar{\nu}_\tau$) neutrinos for the MMHT2014 (top) and NNPDF30 (bottom) sets of collinear PDFs for the leading (left) and subleading (right) D_s -meson production mechanisms. Contributions from the direct and the chain decay modes are shown separately. Further details are specified in the figure.

Similar conclusions as above can be drawn from the analysis of the neutrino (antineutrino) laboratory frame energy distributions shown in Fig. 12. The direct decay mode dominates for smaller energies while the chain mode for larger energies. The crosspoint is found to be between 20 – 40 GeV and is slightly different for the leading and for the subleading contributions. The value for the leading contribution is consistent with the results reported in Ref. [8]. The differences of the neutrino distributions obtained with

the MMHT2014 and the NNPDF30 PDFs for the leading and the subleading mechanisms are driven by the respective differences of the D_s -meson distributions (see the discussion of Fig. 6).

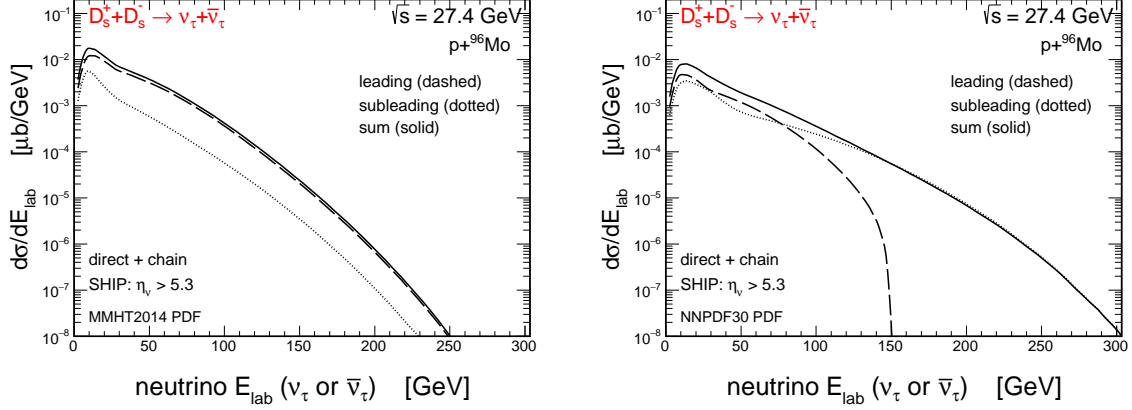


FIG. 13: Laboratory frame energy distributions of ν_τ (or $\bar{\nu}_\tau$) neutrinos for MMHT2014 (left) and NNPDF30 (right) sets of collinear PDFs produced in $p + {}^{96}\text{Mo}$ collisions. Here we show in the same panel the leading and subleading contributions as well as their sum. Contributions from the direct and chain decays are added together. Further details are specified in the figure.

In analogy to Fig. 6, where the laboratory frame energy distributions of the D_s meson are shown, here we wish to present similar distributions but for the neutrinos/antineutrinos. In Fig. 13 we show the impact of the subleading contribution for the predictions of ν_τ and/or $\bar{\nu}_\tau$ energy distributions for the SHiP experiment. Again we obtain two different scenarios for the two different PDF sets. The MMHT2014 PDFs set leads to an almost negligible subleading contribution in the whole energy range while the NNPDF30 PDFs set provides the subleading contribution to be dominant at larger energies ($E_{\text{lab}} > 100$ GeV). If such distributions could be measured by the SHiP experiment then they could be useful to constrain the PDFs in the purely known kinematical region.

B. Number of neutrinos/antineutrinos observed for the Pb target

The calculated previously distributions are a bit theoretical. In this subsection we wish to make relations to what can be observed in the experiment. As discussed previously the neutrino/antineutrino interaction with the matter is strongly energy dependent.

In Fig.14 we show the integrand of the integral in Eq.(2.10). This can be interpreted as a number of produced neutrinos/antineutrinos per interval of (laboratory) energy. As seen in the figure, the distributions corresponding to the direct production are peaked at $E_{\text{lab}} \approx 20$ GeV. For the chain neutrinos the situation strongly depends on the gluon distribution for the leading contribution and on $s(x)/\bar{s}(x)$ distributions for the subleading contributions. The latter ones are, however, much less certain and a better understanding of the $s \rightarrow D_s$ transition is required. The maximum of the chain contributions is at $E_{\text{lab}} \sim 50\text{-}100$ GeV and depends on the details of the model. The discussed measurement can be therefore used to verify the existing parton distributions. An extraction of gluon distributions seems, however, difficult.

After integrating the above integrands one gets numbers of neutrinos/antineutrinos collected in Table III. Quite different numbers are obtained for the different considered scenarios. We get larger numbers than in Ref. [8] but smaller than in Ref. [7]. The chain contribution is significantly larger (about factor 7) than the direct one. For the MMHT2014 distribution the contribution of the leading mechanism is much larger than for the subleading one. For the NNPDF30 distributions the situation is reversed. We predict large observation asymmetry (see the last column) for ν_τ and $\bar{\nu}_\tau$. This asymmetry is bigger than shown e.g. in Refs. [7, 8]. This is due to the subleading mechanism for D_s^\pm meson production included in the present paper. The observation asymmetry for the leading contribution which comes from the differences of the ν_τ and $\bar{\nu}_\tau$ interactions with target are estimated at the level of 50%. In the case of the subleading contribution the asymmetry increases to 60-70%, depending on PDF model.

Finally, in Fig. 15 we show asymmetry in the production of ν_τ and $\bar{\nu}_\tau$ defined as follows:

$$A(E_{\text{lab}}) = \frac{d\sigma_{\nu_\tau}/dE_{\text{lab}} - d\sigma_{\bar{\nu}_\tau}/dE_{\text{lab}}}{d\sigma_{\nu_\tau}/dE_{\text{lab}} + d\sigma_{\bar{\nu}_\tau}/dE_{\text{lab}}}, \quad (3.1)$$

for the sum of the leading and subleading production mechanisms. Here we have included both the direct and chain contributions. Particularly large positive asymmetry is observed in the case of the NNPDF30 PDF set due to the relative large contribution of the subleading mechanism as compared to the case of the MMHT2014 PDF. We conclude that the asymmetry may strongly depend on the parton distributions used in the calculations. Therefore we think that the SHiP experiment will be able to verify the latter.

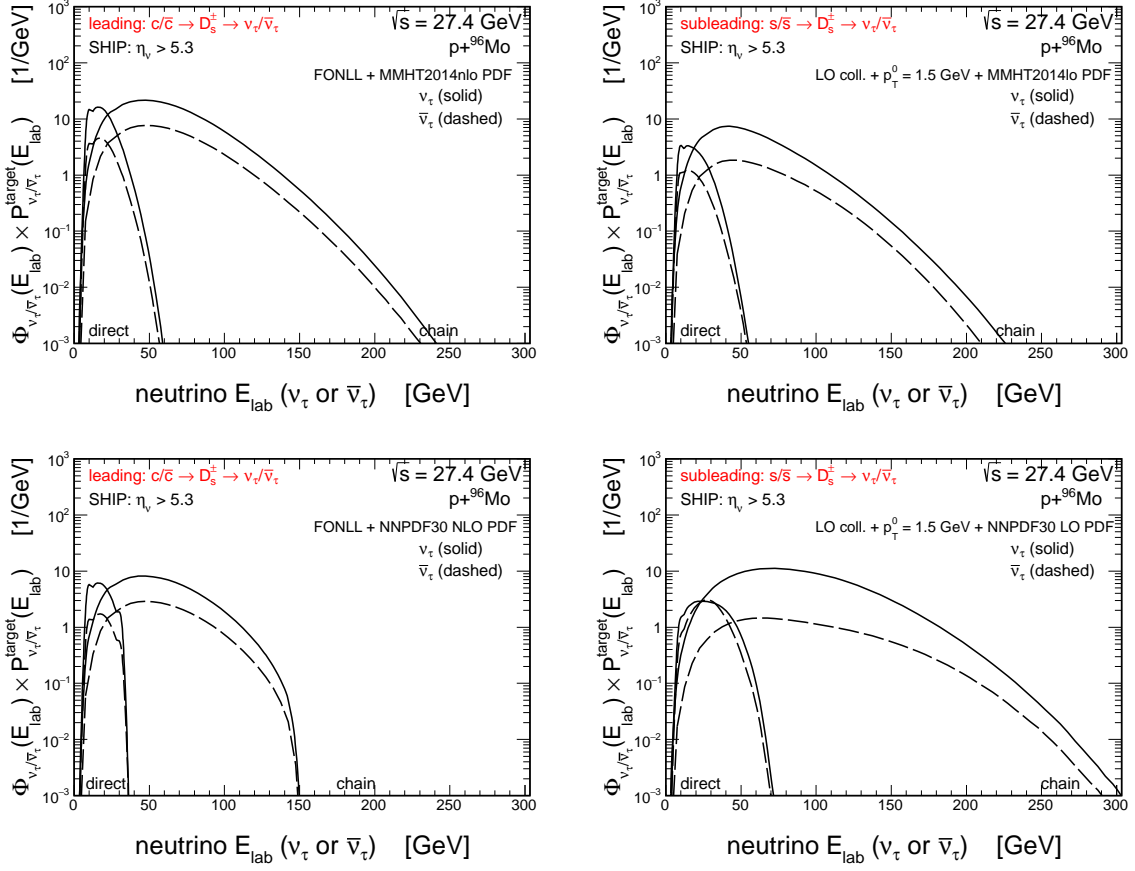


FIG. 14: Integrand of Eq.(2.10) for the MMHT2014 (top) and the NNPDF30 (bottom) sets of collinear PDF for the leading (left) and subleading (right) mechanisms of D_s meson production. We show results for ν_{τ} (solid) and $\bar{\nu}_{\tau}$ (dashed) separately for both the direct and chain contributions.

TABLE III: Number of observed ν_τ and $\bar{\nu}_\tau$ for the SHiP experiment.

Framework/mechanism	Number of observed neutrinos				
	flavour	direct	chain	$\nu_\tau + \bar{\nu}_\tau$	$\frac{\nu_\tau - \bar{\nu}_\tau}{\nu_\tau + \bar{\nu}_\tau}$
FONLL + NNPDF30 NLO PDF $c/\bar{c} \rightarrow D_s^\pm \rightarrow \nu_\tau/\bar{\nu}_\tau$	ν_τ	96	515	818	0.49
	$\bar{\nu}_\tau$	27	180		
LO coll. + NNPDF30 LO PDF $s/\bar{s} \rightarrow D_s^\pm \rightarrow \nu_\tau/\bar{\nu}_\tau$	ν_τ	93	1092	1416	0.67
	$\bar{\nu}_\tau$	75	156		
FONLL + MMHT2014nlo PDF $c/\bar{c} \rightarrow D_s^\pm \rightarrow \nu_\tau/\bar{\nu}_\tau$	ν_τ	277	1427	2292	0.49
	$\bar{\nu}_\tau$	80	508		
LO coll. + MMHT2014lo PDF $s/\bar{s} \rightarrow D_s^\pm \rightarrow \nu_\tau/\bar{\nu}_\tau$	ν_τ	59	435	632	0.56
	$\bar{\nu}_\tau$	21	117		

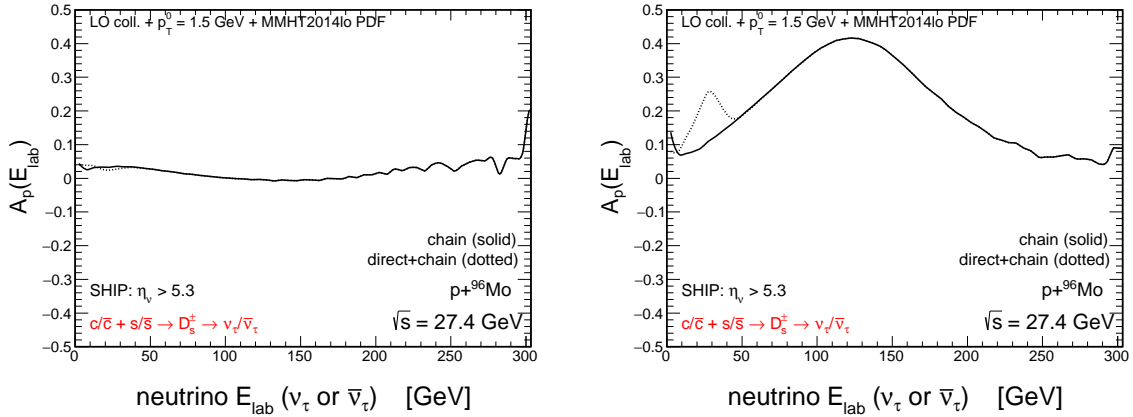


FIG. 15: The production asymmetry $A(E_{\text{lab}})$ as a function of neutrino/antineutrino laboratory frame energy for the MMHT2014 PDFs (left panel) and the NNPDF30 PDFs (right panel) for the sum of the leading and subleading mechanisms for D_s meson production. Both the direct and chain contributions are included.

IV. CONCLUSIONS

In the present paper we have discussed the mechanism and cross sections for production of ν_τ and $\bar{\nu}_\tau$ in fixed target experiment for $\sqrt{s_{NN}} = 27.4$ GeV with 400 GeV proton beam and molybdenum target. In the present analysis we have assumed that the neutrinos/antineutrinos are produced exclusively from D_s^\pm mesons. Other, probably small, contributions (Drell-Yan, $\gamma\gamma$ fusion, B decays, etc.) have been neglected here.

We include two different contributions of D_s meson production: the leading fragmentation of c and \bar{c} and the subleading fragmentation of s and \bar{s} . The cross section for c/\bar{c} production has been obtained either using the FONLL framework or in the k_T -factorization approach using the Kimber-Martin-Ryskin unintegrated parton distributions. The s and \bar{s} production cross sections have been calculated here in the leading-order collinear factorization approach with on-shell initial state partons and with a special treatment of minijets at low transverse momenta, as adopted *e.g.* in PYTHIA.

The neutrinos are produced then via the direct decay mode $D_s^\pm \rightarrow \tau^\pm \nu_\tau / \bar{\nu}_\tau$ and via the chain decay of τ^+ or τ^- leptons. The direct production is very simple as pseudoscalar (spin zero) D_s mesons decay isotropically in its rest frame. The chain decay is more involved technically. In the present paper we have used TAUOLA package to generate sequential τ decays. All decay channels implemented in TAUOLA have been included in the calculation. The four-momenta of $\nu_\tau/\bar{\nu}_\tau$ in the τ rest frame have been transformed event-by-event to the proton-nucleon center-of-mass system or laboratory frame using relevant Lorentz transformations and then corresponding distributions have been constructed.

The cross section for $p + {}^{96}\text{Mo}$ was obtained from that for the proton-proton or proton-neutron collisions via a simple counting of individual pp and pn collisions. We have taken the well known probabilities of $c \rightarrow D_s$ fragmentation and branching fraction for the $D_s \rightarrow \nu_\tau + \tau$ decay.

We have presented resulting distributions of neutrinos/antineutrinos in transverse momentum and laboratory energy. Such distributions are crucial to calculate interactions of ν_τ and $\bar{\nu}_\tau$ with the lead target. We have presented also production asymmetry for ν_τ and $\bar{\nu}_\tau$ as a function of neutrino/antineutrino energy.

In the present paper we have included also subleading (unfavored) fragmentation

($s \rightarrow D_s^-$ or $\bar{s} \rightarrow D_s^+$). In principle, when $s(x) \neq \bar{s}(x)$ such a subleading mechanism could lead to different distributions of D_s^+ and D_s^- and in the consequence different distributions of ν_τ and $\bar{\nu}_\tau$.

The subleading fragmentation leads to asymmetry provided s and \bar{s} distributions are different. We have discussed a possible role of the subleading production of D_s mesons in the context of “increasing” the production of $\nu_\tau/\bar{\nu}_\tau$ neutrino/antineutrino at the SHiP experiment. A similar effect for production of high-energy $\nu_\tau/\bar{\nu}_\tau$ neutrinos/antineutrinos was discussed very recently in Ref. [13]. The subleading fragmentation may increase the probability of observing $\nu_\tau/\bar{\nu}_\tau$ neutrinos/antineutrinos by the planned SHiP fixed target experiment at CERN. We have found that present knowledge of s/\bar{s} parton distributions and especially s/\bar{s} fragmentation to D_s mesons does not allow for precise estimations. The SHiP experiment could be therefore useful to test s/\bar{s} distributions.

Acknowledgments

This study was partially supported by the Polish National Science Center grant UMO-2018/31/B/ST2/03537 and by the Center for Innovation and Transfer of Natural Sciences and Engineering Knowledge in Rzeszów. We are indebted to Adam Kozela, Jacek Otwinowski, Jan Sobczyk and Agnieszka Zalewska for discussion on some issues presented in this paper. We are particularly indebted to Jan Sobczyk for his help in using the NuWro computer program.

-
- [1] K. Kodama *et al.* [DONUT Collaboration], Phys. Lett. B **504**, 218 (2001).
 - [2] K. Kodama *et al.* [DONuT Collaboration], Phys. Rev. D **78**, 052002 (2008).
 - [3] N. Agafonova *et al.* [OPERA Collaboration], Phys. Rev. Lett. **120**, no. 21, 211801 (2018) Erratum: [Phys. Rev. Lett. **121**, no. 13, 139901 (2018)].
 - [4] IceCube Collaboration, private communications,
 - [5] M. Anelli *et al.* [SHiP Collaboration], arXiv:1504.04956 [physics.ins-det].
 - [6] S. Alekhin *et al.*, Rept. Prog. Phys. **79**, no. 12, 124201 (2016).
 - [7] A. Buonauro [SHiP Collaboration], PoS DIS **2016**, 260 (2016) [arXiv:1609.04860 [physics.ins-det]].
 - [8] W. Bai and M. H. Reno, J. High Energy Phys. **02**, 077 (2019).

- [9] M. Tanabashi *et al.* [Particle Data Group], Phys. Rev. D **98**, no. 3, 030001 (2018).
- [10] B. Abelev *et al.* [ALICE Collaboration], Phys. Lett. B **718**, 279 (2012).
- [11] R. Aaij *et al.* [LHCb Collaboration], Nucl. Phys. B **871**, 1 (2013).
- [12] R. Aaij *et al.* [LHCb Collaboration], J. High Energy Phys. **08**, 008 (2018).
- [13] V. P. Goncalves, R. Maciuła and A. Szczurek, Phys. Lett. B **794**, 29 (2019).
- [14] Yu.S. Jeong and M.H. Reno, Phys. Rev. **D82** (2010) 033010.
- [15] M. Cacciari, *et al.*, J. High Energy Phys. **10** (2012) 137 [arXiv:1205.6344 [hep-ph]].
- [16] R. Maciuła and A. Szczurek, arXiv:1905.06697 [hep-ph].
- [17] M. Cacciari, M. Greco and P. Nason, J. High Energy Phys. **05** (1998) 007;
M. Cacciari, S. Frixione and P. Nason, J. High Energy Phys. **03** (2001) 006.
- [18] S. Catani, M. Ciafaloni and F. Hautmann, Phys. Lett. B **242** (1990) 97; Nucl. Phys. B **366** (1991) 135; Phys. Lett. B **307** (1993) 147; J.C. Collins and R.K. Ellis, Nucl. Phys. B **360**, 3 (1991); L.V. Gribov, E.M. Levin, and M.G. Ryskin, Phys. Rep. **100**, 1 (1983); E.M. Levin, M.G. Ryskin, Yu.M. Shabelsky and A.G. Shuvaev, Sov. J. Nucl. Phys. **53**, 657 (1991).
- [19] M. Epele, C. Garca Canal and R. Sassot, Phys. Lett. B **790**, 102 (2019).
- [20] T. Kneesch, B. A. Kniehl, G. Kramer and I. Schienbein, Nucl. Phys. B **799**, 34 (2008).
- [21] T. Sjöstrand *et al.*, Comput. Phys. Commun. **191**, 159 (2015).
- [22] R. Maciuła and A. Szczurek, Phys. Rev. D **97**, no. 7, 074001 (2018).
- [23] L. A. Harland-Lang, A. D. Martin, P. Motylinski and R. S. Thorne, Eur. Phys. J. C **75**, no. 5, 204 (2015).
- [24] R. D. Ball *et al.* [NNPDF Collaboration], J. High Energy Phys. **04**, 040 (2015).
- [25] P. Jimenez-Delgado and E. Reya, Phys. Rev. D **89**, no. 7, 074049 (2014).
- [26] R. Maciuła and A. Szczurek, arXiv:1907.13388 [hep-ph].
- [27] V. Bertone *et al.* [NNPDF Collaboration], Eur. Phys. J. C **77**, no. 8, 516 (2017).
- [28] G. Watt, A. D. Martin and M. G. Ryskin, Phys. Rev. D **70**, 014012 (2004) Erratum: [Phys. Rev. D **70**, 079902 (2004)]
- [29] S. Dulat *et al.*, Phys. Rev. D **93**, no. 3, 033006 (2016).
- [30] A. Bermudez Martinez, P. Connor, H. Jung, A. Lelek, R. Iebk, F. Hautmann and V. Radescu, Phys. Rev. D **99**, no. 7, 074008 (2019).
- [31] P. Renton, Cambridge, UK: Univ. Pr. (1990) 596 p
- [32] S. M. Barr, T. K. Gaisser, P. Lipari and S. Tilav, Phys. Lett. B **214**, 147 (1988).

- [33] T. K. Gaisser, Cambridge, UK: Univ. Pr. (1990) 279 p
- [34] L. Pasquali and M. H. Reno, Phys. Rev. D **59**, 093003 (1999).
- [35] S. Jadach, J. H. Kuhn and Z. Wąs, Comput. Phys. Commun. **64**, 275 (1990).
M. Jeżabek, Z. Wąs, S. Jadach and J. H. Kuhn, Comput. Phys. Commun. **70**, 69 (1992).
S. Jadach, Z. Wąs, R. Decker and J. H. Kuhn, Comput. Phys. Commun. **76**, 361 (1993).
M. Chrzaszcz, T. Przędziński, Z. Wąs and J. Zaremba, Comput. Phys. Commun. **232**, 220 (2018).
- [36] B. B. Abelev *et al.* [ALICE Collaboration], Phys. Rev. Lett. **113**, no. 23, 232301 (2014).
- [37] J. Żmuda, K. M. Graczyk, C. Juszczak and J. T. Sobczyk, Acta Phys. Polon. B **46**, no. 11, 2329 (2015).
- [38] H. Dijkstra and T. Ruf (SHiP collaboration), "Heavy Flavour Cascade Production in a Beam Dump", CERN-SHiP-NOTE-2015-009.